

2021

A review of enhancement of biohydrogen productions by chemical addition using a supervised machine learning method

Yiyang Liu

Jinze Liu

Hongzhen He

Shanru Yang

Yixiao Wang

See next page for additional authors

Follow this and additional works at: <https://ro.ecu.edu.au/ecuworkspost2013>



Part of the [Engineering Commons](#)

[10.3390/en14185916](https://ro.ecu.edu.au/ecuworkspost2013/11175)

Liu, Y., Liu, J., He, H., Yang, S., Wang, Y., Hu, J., . . . Sun, Y. (2021). A review of enhancement of biohydrogen productions by chemical addition using a supervised machine learning method. *Energies*, 14(18), article 5916.

<https://doi.org/10.3390/en14185916>

This Journal Article is posted at Research Online.

<https://ro.ecu.edu.au/ecuworkspost2013/11175>

Authors

Yiyang Liu, Jinze Liu, Hongzhen He, Shanru Yang, Yixiao Wang, Jin Hu, Huan Jin, Tianxiang Cui, Gang Yang, and Yong Sun

Review

A Review of Enhancement of Biohydrogen Productions by Chemical Addition Using a Supervised Machine Learning Method

Yiyang Liu ^{1,†}, Jinze Liu ^{1,†}, Hongzhen He ¹, Shanru Yang ², Yixiao Wang ¹, Jin Hu ¹, Huan Jin ^{3,*}, Tianxiang Cui ³, Gang Yang ⁴ and Yong Sun ^{1,5,*}

- ¹ Key Laboratory of Carbonaceous Wastes Processing and Process Intensification of Zhejiang Province, University of Nottingham Ningbo, Ningbo 315100, China; yiyangliu0904@163.com (Y.L.); jinze_lau@163.com (J.L.); Hongzhen.he20@imperial.ac.uk (H.H.); shyyw12@nottingham.edu.cn (Y.W.); ssyjh3@nottingham.edu.cn (J.H.)
- ² Centre for English Language Education (CELE), University of Nottingham Ningbo, Ningbo 315100, China; shanru.yang@nottingham.edu.cn
- ³ School of Computer Science, University of Nottingham Ningbo, Ningbo 315100, China; tianxiang.cui@nottingham.edu.cn
- ⁴ Institute of Process Engineering, Chinese Academy of Sciences, Beijing 100864, China; yanggang@ipe.ac.cn
- ⁵ School of Engineering, Edith Cowan University, 70 Joondalup Drive, Perth, WA 6027, Australia
- * Correspondence: huan.jin@nottingham.edu.cn (H.J.); y.sun@ecu.edu.au or yong.sun@nottingham.edu.cn (Y.S.)
- † Authors have equal contributions.



Citation: Liu, Y.; Liu, J.; He, H.; Yang, S.; Wang, Y.; Hu, J.; Jin, H.; Cui, T.; Yang, G.; Sun, Y. A Review of Enhancement of Biohydrogen Productions by Chemical Addition Using a Supervised Machine Learning Method. *Energies* **2021**, *14*, 5916. <https://doi.org/10.3390/en14185916>

Academic Editor: Bahman Shabani

Received: 25 August 2021

Accepted: 14 September 2021

Published: 17 September 2021

Publisher's Note: MDPI stays neutral with regard to jurisdictional claims in published maps and institutional affiliations.



Copyright: © 2021 by the authors. Licensee MDPI, Basel, Switzerland. This article is an open access article distributed under the terms and conditions of the Creative Commons Attribution (CC BY) license (<https://creativecommons.org/licenses/by/4.0/>).

Abstract: In this work, the impact of chemical additions, especially nano-particles (NPs), was quantitatively analyzed using our constructed artificial neural networks (ANNs)-response surface methodology (RSM) algorithm. Fe-based and Ni-based NPs and ions, including Mg^{2+} , Cu^{2+} , Na^+ , NH_4^+ , and K^+ , behave differently towards the response of hydrogen yield (HY) and hydrogen evolution rate (HER). Manipulating the size and concentration of NPs was found to be effective in enhancing the HY for Fe-based NPs and ions, but not for Ni-based NPs and ions. An optimal range of particle size (86–120 nm) and Ni-ion/NP concentration ($81\text{--}120\text{ mg L}^{-1}$) existed for HER. Meanwhile, the manipulation of the size and concentration of NPs was found to be ineffective for both iron and nickel for the improvement of HER. In fact, the variation in size of NPs for the enhancement of HY and HER demonstrated an appreciable difference. The smaller (less than 42 nm) NPs were found to definitely improve the HY, whereas for the HER, the relatively bigger size of NPs (40–50 nm) seemed to significantly increase the H_2 evolution rate. It was also found that the variations in the concentration of the investigated ions only statistically influenced the HER, not the HY. The level of response (the enhanced HER) towards inputs was underpinned and the order of significance towards HER was identified as the following: $Na^+ > Mg^{2+} > Cu^{2+} > NH_4^+ > K^+$.

Keywords: biohydrogen ($BioH_2$); nanoparticles; quantitative assessment; artificial neuron networks; process intensifications

1. Introduction

The further rollback of globalization will ultimately reshape the current supply chain block, especially as more and more countries have realized how pivotal it is to have self-sufficient industries to produce strategic products such as medicine, energy, and even toilet paper rolls [1]. Aside from the public health emergency, energy security is another draconian challenge that countries across the world are reluctantly facing, although the price of crude oil did once plunge to USD 25 per barrel (158.98 L) in the middle of 2020 during the COVID-19 pandemic [2]. Whether to take bolder steps in the energy reliance transition from fossil fuel to renewable energy will make a great difference in the world that our children will be able to inherit in the future [3]. Consequently, by 2021, several

developed countries already started to restrict the use of fossil fuels in order to eventually achieve a shift in fuel type [4,5].

Among all sources of energy, hydrogen (H_2) is one of the most favorable candidates due to its inherent appealing features: (1) high energy yield (122 kJ kg^{-1}), (2) generation of water as a result of combustion, and (3) electricity generation through the fuel cell [6,7]. However, the current predominant H_2 generation still comes from fossil-based materials via existing mature industrial chemical processes such as natural gas steam reforming (NGSR), nature gas thermal cracking (NGTC), auto-thermal reforming (ATR), coal gasification, and partial oxidation of heavier-than-naphtha hydrocarbons [8]. Consequently, the paradox of sustainability of H_2 utilization and the non-renewability of H_2 generation will be encountered, although the development of carbon capture storage and utilization (CCSU) such as via a mature catalytic process like Fischer–Tropsch synthesis might alleviate environmental impacts from H_2 generation [9–12].

Apart from the thermal process, the biological hydrogen ($BioH_2$) generation process also plays a supplementary role in H_2 generation due to features such as versatile feedstock (lignocellulose, wet kitchen organic waste, and wastewater) and no green-house gas emissions (GHE). Despite the appealing advantages that are mentioned above, $BioH_2$ production is hampered by its relatively lower process performance [13]. To implement $BioH_2$ in different applications either on a decentralized or centralized basis or both, different process intensification approaches have been proposed, such as hydrolysate detoxification, mixed continuous and batch operations, co-fermentation, process optimization, and chemical addition. Among these approaches, chemical addition is considered to be one of the most attractive and practical ones because of its operational simplicity (without any additional modifications) and relatively low energy consumption [14]. However, current reports are limited to focusing on the facilitation of $BioH_2$ production by all types of chemical additives. In contrast, the nanoparticles (NPs) as a potential type of chemical additive still lack research on their addition and the corresponding quantitative relationships, such as hydrogen yield (HY) and hydrogen evolution rate (HER) with detailed incubation conditions, especially the concentration of different metal elements.

In this paper, instead of making a simple $BioH_2$ production enhancement comparison using the addition of NPs across literature reports, the collected data (such as HY, HER, and the substrate concentrations from literature works) were used to construct the data matrix for supervised machine learning algorithm using the developed artificial neural networks (ANNs) coupled with statistical analysis using response surface methodology (RSM) for more insightful and quantitative correlations and analysis. The review of assessing the impact of NPs additions on $BioH_2$ production in form of HY and HER using a developed ANNs-RSM algorithm, to the best of our knowledge, has not been reported before.

2. Materials and Methods

The literature used in this review was mainly collected from the scientific databases from Web of Science, Google Scholar and Science Direct via keyword search. Various keyword groups were comprised of several words, including “dark fermentation,” “biohydrogen,” and “nanoparticles.” With regard to the possible missing relevant literature, by using the abovementioned searching strategy, an extensive additional search process was conducted with more detailed keywords, including “trace metal,” “transitional metal,” “iron,” “nickel,” “gold,” “copper,” and “metal oxide.” During the additional search, these mentioned keywords were also combined with the keyword “biohydrogen.”

The ANNs (based on Python 2.7 platform) was deployed for data analysis. The detailed schematic diagram of the construction of the ANNs and data collection is shown in Figure S1. In this work, the widely used feed-forward three-layer networks were used. The simplified cross-out method was used for cross-validation during the data training step. The detailed descriptions of the standard procedures for this methodology can be

found in our previous works [15]. During the data training, the mean square error (*MSE*) and mean average relative residual (*MARR*) were computed as follows:

$$MSE\% = \frac{1}{N_{sam}} \sum_{j=1}^{N_{sam}} (r_i^{sam} - r_i^{cal})^2 \times 100\% \quad (1)$$

$$MARR\% = \frac{1}{N_{sam}} \sum_{j=1}^{N_{sam}} \left(\frac{|r_i^{sam} - r_i^{cal}|}{r_i^{sam}} \right) \times 100\% \quad (2)$$

where N_{sam} is the number of data, and r_i^{sam} and r_i^{cal} are actual and calculated values, respectively. The setting for allowable accuracy was 95%. For the ANNs prediction data matrix, the widely used Box–Behnken design (BBD) and the central composite design (CCD) were used to predict the data matrix generation [16]. Once the supervised data learning was complete, the analysis of variation (ANOVA) based on commercial Design Expert[®] Version 11 software package (Stat-Ease, Inc., Minneapolis, MN, USA) was used for statistical analysis.

3. Literature Survey Comparisons

In this paper, for the convenience of discussion, four different types of NPs (Fe-based, Au-based, Cu-based, and Ni-based) were surveyed across different studies and the results are shown in Figure 1.

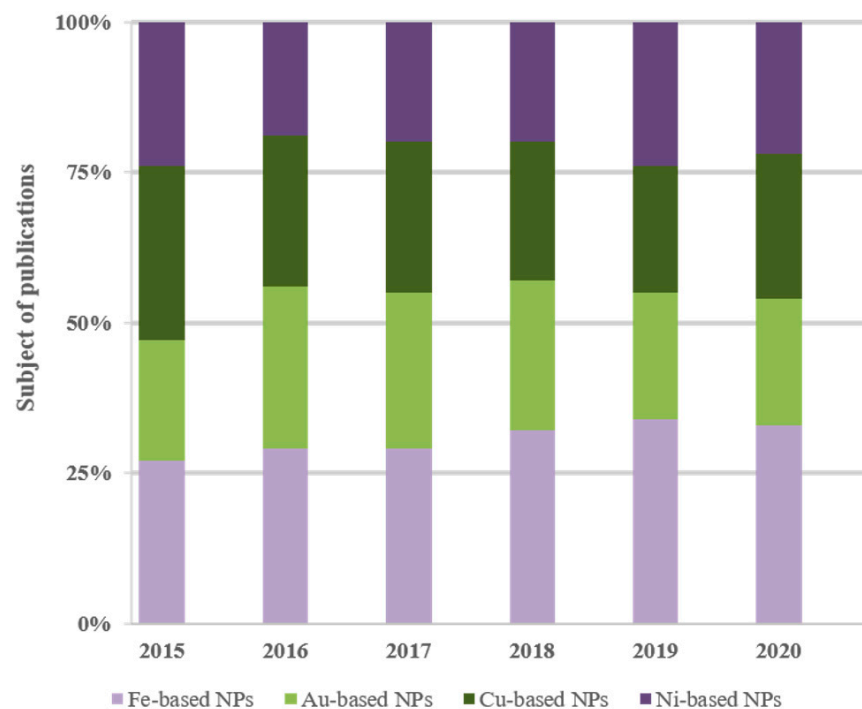


Figure 1. Statistics of publications from Scopus and Google Scholar in regard to BioH₂ production by chemical nanoparticle additions.

For each type of NPs, taking Ni-based NPs, for instance, all nickel-related species were included, such as nanoparticles such as zero-valent particles, metal oxide NiO₂, etc. The number of reports on the topic of BioH₂ enhancement by NPs additions has been increasing steadily since 2015. Among different NPs, the number of reports using iron-based NPs has presented a discernible trend in recent years. The impetus underlining this trend is possibly associated with its inherent appealing cost-effective feature compared to other NPs such as gold or nickel. Apart from Fe-based NPs, Ni-based NPs have experienced an appreciable increase in recent years, with an exception in 2015 [17,18]. The research interests that focus

on Ni-based NPs might be pertinent to the metal cluster of hydrogenase [19]. According to recent classifications, there are three different hydrogenases, namely, [Fe], [NiFe], and [FeFe] [20,21]. During biological chemical reactions, these enzyme active centers play a pivotal role in the metabolism of proton ion-associated redox reactions. Studies have shown that [FeFe] hydrogenase catalyzes H_2 generation, whereas [NiFe] hydrogenase catalyzes the consumption of H_2 . [NiFe] hydrogenase presents a relatively higher tolerance to the existence of oxygen and it widely exists in various types of microbial strains, whereas [FeFe] hydrogenase is relatively strict to the presence of oxygen and only exists in some algae and bacteria [22,23]. Regarding [Fe] hydrogenase, it only strictly exists in some methanogen strains [24–26].

4. Underlying Mechanisms of Metal Ions and Metal-Based Nanoparticles

Many extensively studied metal ions and metal-based nanoparticles are regarded as effective additives in culture medium to facilitate $BioH_2$ production in the dark fermentation process, including Na^+ , K^+ , NH_4^+ , Mg^{2+} , Ca^{2+} , Co^{2+} , Zn^{2+} , Cu^{2+} , Fe^{2+}/Fe^{3+} , and Ni^{2+}/Ni^{3+} , among others [27–29]. Extensive studies have found that even small changes in the latter may have a significant impact on $BioH_2$ production; hence, many strategies have been proposed based on them, such as concentration regulation, including concentration manipulation [30], size regulation [17,31], composites fabrication [23,32], and heteroatom doping [33]. In general, the enhancement of NPs addition lies in a few important facts: (i) the controllable release of metal ions that facilitates the passive transport across the membrane [34]; (ii) nanodots that facilitate the electron transport chain during metabolism, such as glycolysis [35]; and (iii) the appropriate level of NPs favorable to the hydrogenase activities (co-enzymes often contain the metal ions in the catalysis center, which ultimately enhances the rate of hydrogen generation [36]. The potential mechanisms of $BioH_2$ enhancement are summarized in Figure 2. Therefore, in this part, this review will focus on the impact of the latter on $BioH_2$ production and its mechanisms.

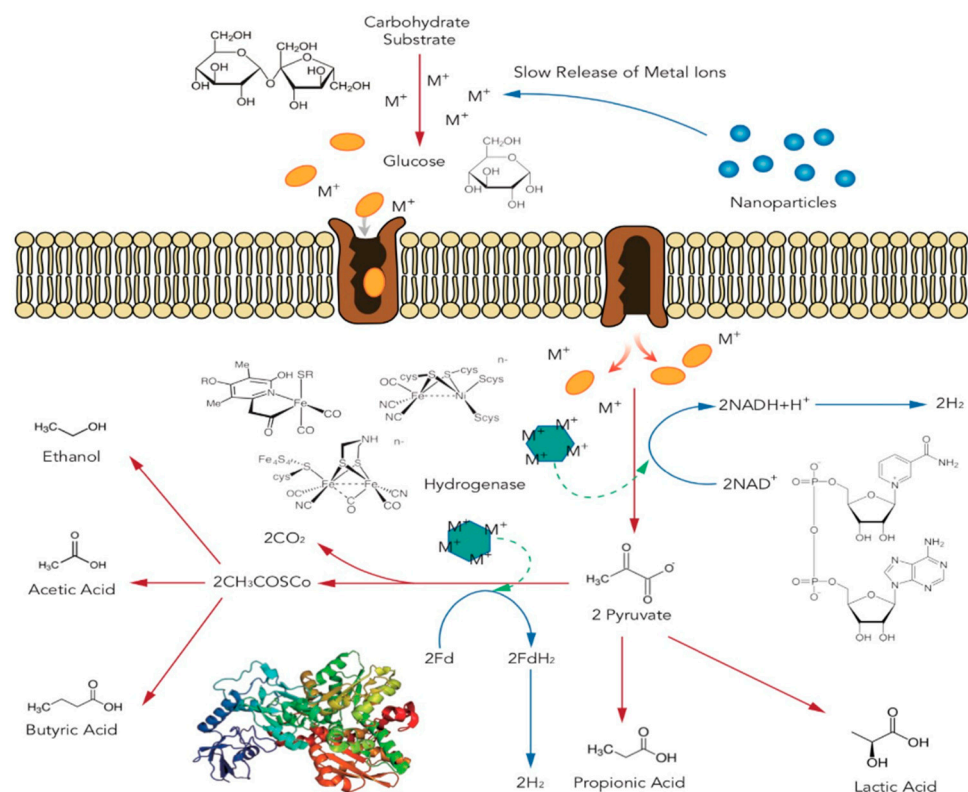


Figure 2. Potential mechanism of $BioH_2$ enhancement by NPs addition.

4.1. Fe-Based Ions and Nanoparticles

Iron is an important trace element in the formation of hydrogenases and other enzymes. The pre-addition of Fe in the culture medium is a widely used strategy to enhance BioH₂ production in dark fermentation [37]. As illustrated in Figure 2, first, Fe is the essential element to form the metal content at the active sites of hydrogenase ([FeFe], [FeNi], and [Fe]), thus catalyzing the reduction reaction of H⁺ to H₂ [38]. Second, the presence of Fe-based NPs improves the activity of ferredoxin oxidoreductase by reducing the dissolved oxygen (DO) level and enhancing electron transfer due to the surface and quantum size effects [39,40]. In addition, Fe-based components could participate in enriching the microbial community and enhancing the growth of H₂-producing bacteria [41]. The oxidative stress increases when there is a higher Fe concentration, which results in the formation of abundant oxidative radicals, thus leading to the deactivation or decomposition of enzymes [17,30].

4.2. Ni-Based Ions and Nanoparticles

Similarly, nickel ions or Ni-based nanoparticles are another widely studied substance that can significantly enhance BioH₂ production in dark fermentation. The mechanisms between Ni-ion/Ni-based nanoparticles and Fe-ion/Fe-based nanoparticles are largely identical but with minor differences. The key mechanisms for Ni include (a) facilitating the synthesis of [FeNi] hydrogenase [42], (b) improving the activity of ferredoxin oxidoreductase [43], and (c) Ni NPs controlling the concentration of Ni²⁺ at the optimum level. In addition, it is worth noting that [NiFe] hydrogenase exists in more bacteria than [FeFe] hydrogenase. Therefore, Ni can promote H₂-producing bacteria in the dark fermentation process to a certain extent [44].

5. Results

5.1. Impact of Fe-Based Ions and NP Addition

To quantitatively unveil the impact of the concentration of Fe-ion/Fe NPs and size effects upon the HY and HER in BioH₂ generation, the collected values from the literature (Table 1) were statistically analyzed through our previously established ANN-RSM method and the results are shown in Figure 3.

Table 1. Comparison of BioH₂ production with the addition of Fe-based nanoparticles.

NPs	Opt/mg L ⁻¹	Substrate	SC/g L ⁻¹	Size/nm	HY/mmol g ⁻¹	HER/mmol L ⁻¹ h ⁻¹	Reference
Fe (NPs)	400	Grass	10.7	50	2.9	5.4	[45]
Fe (NPs)	25	Starch	5	35	3	-	[18]
Fe (NPs)	300	Malate	3	16	20	0.4	[46]
Fe (NPs)	50	Xylose	30	75	13.3	2	[47]
Fe (NPs)	200	MSJ	10	50	0.9	2.4	[48]
Fe (NPs)	200	Sucrose	7.5	50	15.9	10.1	[27]
Fe (NPs)	175	Glucose	7.5	59	12.9	5.69	[28]
Fe (NPs)	50	Starch	6	35	5	-	[43]
Fe (NPs)	250	Malate	4	12	24.2	0.8	[44]
Fe ₂ O ₃ (NPs)	50	Glucose	5	50	1.92	2.5	[49]
Fe ₂ O ₃ (NPs)	50	CDW	15.3	33	16.75	102.5	[17]
Fe ₂ O ₃ (NPs)	200	DW	56	23	7.85	62.4	[30]
Fe ₂ O ₃ (NPs)	50	Wastewater	110	6.5	1.9	49.4	[50]
Fe ₂ O ₃ (NPs)	200	MEG	4	100	8.4	0.6	[51]
Fe ₂ O ₃ (NPs)	300	CAS	10	20	3.875	1.92	[52]
Fe ₂ O ₃ (NPs)	200	Glucose	10	20	9.2	3.1	[52]
Fe ₂ O ₃ (NPs)	60	Glucose	6	60	1.92	2.5	[49]
Fe ₃ O ₄ (NPs)	10	Glucose	2.5	100	10.1	0.23	[53]
Fe ₃ O ₄ (A-C-NPs)	250	Glucose	5	30	11.656	3.2	[38]
GT-INP (Fe ₂ O ₄ and FeO(OH)(NPs)	1000	CO	1.008	70	1.58	0.0662	[54]
Magnetite (NPs)	200	SJ	3	50	6.7	0.23	[55]
Hematite (NPs)	200	Sucrose	12.5	55	10.4	6	[56]

In this table, MEG refers to mono ethylene glycol, SC refers to substrate concentration, MSJ denotes Marcoalgea Saccharina Japonica, NMBL refers to *R. sphaeroides* NMBL-02 and *E. coli* NMBL-04, MC refers to mixed consortia, BA refers to *Bacillus anthracis* PUNAJAN 1, CP refers to *C. pasteurianum*, EA refers to *E. aerogenes* ATCC13408, EC refers to *E. cloacae*, Cl refers to Clostridium, Ca refers to *C. acetobutylicum* NCIM 2337, SJ refers to sugarcane juice, CAS refers to cassava starch.

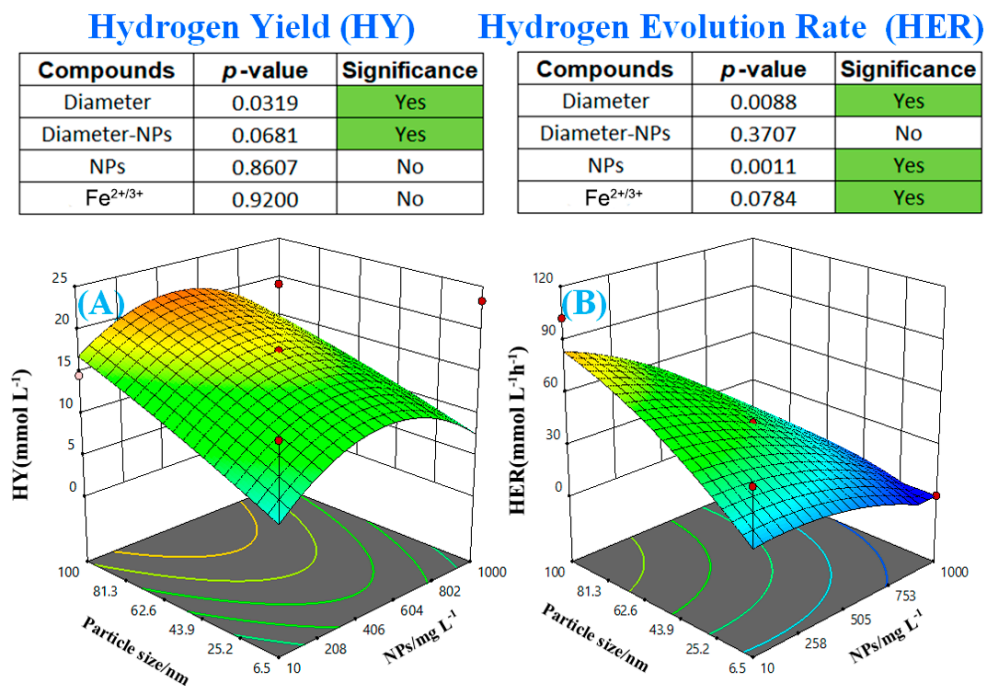


Figure 3. Statistical analysis of HY and HER. HY refers to H₂ yield; HER refers to the H₂ evolution rate. (A) Particle size and NP concentrations versus HY, (B) particle size and NP concentrations versus HER.

The effects of NPs size and NPs concentration together with the binary combined impact upon the HY and HER were extensively explored. Regarding HY, it was found that the size of the NPs together with the concentration of NPs were both statistically significant to the H₂ yield amongst the surveyed literature's reports of experimental conditions. From Figure 3A, it is indicated that the HY tended to approach the highest value in the range of NP size (81–100 nm) and NP concentration (406–604 mg L⁻¹). For HER, it was found that the size of NPs, the concentration of NPs, and Fe²⁺/Fe³⁺ were all significant to HER. For the combined effects (NP size and concentration), on the other hand, these effects were found to be statistically insignificant to HER. The 3D plot of HER versus NPs size and NPs concentration (Figure 3B) also tended to show the highest region of HER located at the size range of 81–100 nm. Among the collected literature reports, the HER seemed to be more appreciably and directly related to the relatively larger size of the particle, which might be quite contradictory to some findings. This indicates that the manipulation of NPs ideally in size range of 81–100 nm is favorable for both high HY and HER. Reducing the size of NPs could improve the quantum dot effect, thus improving the electron transport. In contrast, the electron transport phenomena in extracellular media during cultivation is quite complicated and some factors such as osmosis condition and the activity of the fermentation broth might be counter-effective to the nanoparticle size effect for enhancing BioH₂ generation. Currently, very few works have been done to elucidate the mechanisms of this size impact upon selective enhancement of HY and HER. From our statistical analysis, a reasonable explanation for the ideal size effect is that the nanoparticle size of 81–100 nm is more thermodynamically stable than NPs with a smaller size during fermentation, since Fe-based NPs with smaller size are easier to agglomerate and form large Fe-based particles and deteriorate the electron transport performance in extracellular conditions. The fabrication of composites (e.g., Fe@graphene) is a promising strategy to enable the stable existence of small-sized nanoparticles; however, it has not been widely investigated.

5.2. Impact of Ni-Based Ions and NP Addition

The impact of Ni-based ions and NPs upon HY and HER is summarized in Table 2 and the statistical analysis results are shown in Figure 4.

Table 2. Comparison of BioH₂ production with the addition of Ni-based nanoparticles.

Nanoparticles	Opt/mg L ⁻¹	Substrate	SC/g L ⁻¹	Size/nm	HY/mmol g ⁻¹	HER/mmol L ⁻¹ h ⁻¹	Reference
Ni (NPs)	5.7	Glucose	14.01	13.6	14.1	11.5	[57]
Ni (NPs)	32	Starch	8	80	2.4	10.3	[18]
Ni (NPs)	60	MEG	4.7	60	1.11	1.5	[23]
Ni (NPs)	10	Glucose	1	25	9.5	30	[32]
Ni (NPs)	1	Glucose	2.5	100	11.7	0.28	[53]
Ni (NPs)	4.3	Glucose	13.92	28	12.7	10.4	[57]
Ni (NPs)	2.5	Glucose	5	42.5	10.8	1.3	[58]
Ni (NPs)	25	Starch	10	40	2.7	11.5	[18]
Ni (NPs)	11	Glucose	2.7	120	1.21	0.22	[59]
NiO (NPs)	20	MEG	4	100	7.25	0.5	[51]
NiO (NPs)	10	CDW	15.3	23	15.7	44.9	[17]
NiO (NPs)	1.5	Wastewater	9.6	23.6	0.5	12	[31]
Ni (NPs)	100	CS	20	50	20	0.27	[60]

In this table, MEG refers to mono ethylene glycol, CS: cornstark.

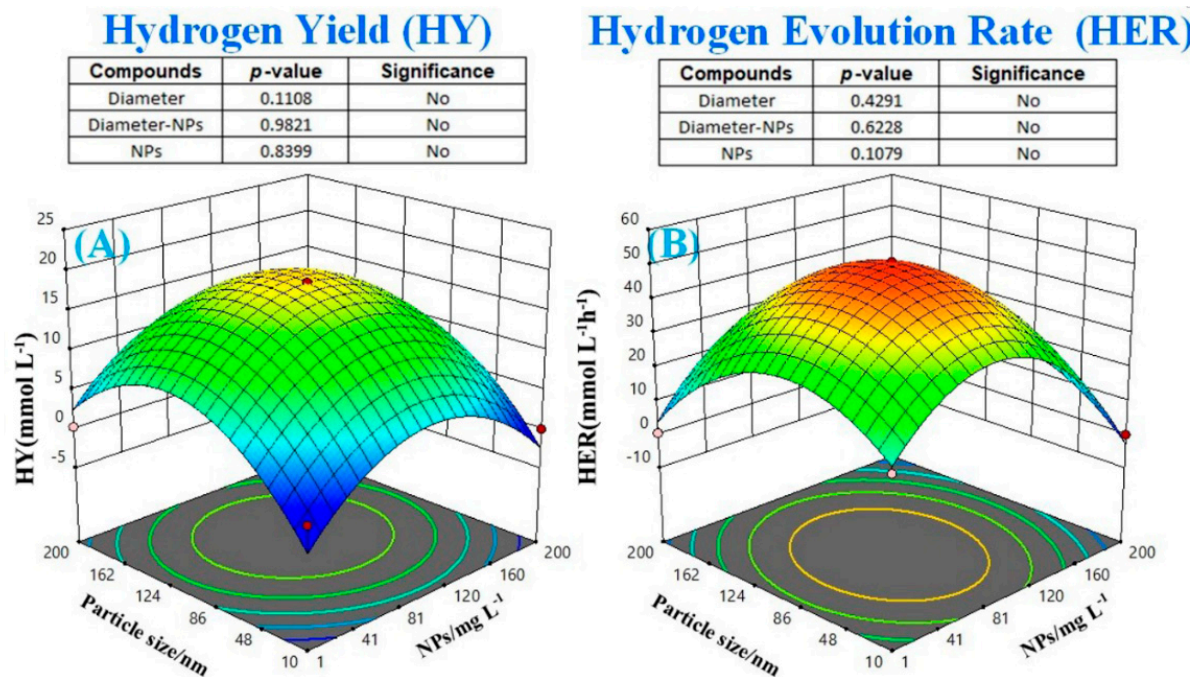


Figure 4. Statistical analysis of HY and HER. (A) Particle size and nanoparticle concentration versus HY, (B) particle size and nanoparticles concentration versus HER.

Among the collected literature reports, the size and concentration of NPs together with their combined effect were not statistically significant to either HY or HER according to the calculated *p*-value. Regarding HY (Figure 4A), it was found that both too low and too high levels of NPs size and concentration were not favorable. Indeed, an optimal range existed if the NP size and concentration were manipulated within 86–120 nm and (81–120 mg L⁻¹, respectively). Similarly, the HER also presented the same variation patterns as those of HY. An optimal range of particle size (86–120 nm) and Ni-ion/NPs concentration (81–120 mg L⁻¹) existed for HER. Unlike Fe, Ni presented more consistent responding patterns between HY and HER in regards to the variation in the size and concentration of NPs. In addition, studies have indicated that Ni-based ions and NPs tend to selectively enhance some BioH₂ generation pathways, such as enhancing the acetate pathway while suppressing or inhibiting butyrate and propionate pathways. However, discrepancies still exist due to different strains of microbes inoculated, cultivation medium, experimental

uncertainties, etc. Although the size of NPs was significant to the HER, the combined effects (NP size and concentration) were found to be insignificant. Among the collected literature reports, the HER seemed to be directly related to the relatively larger size of the particles. This indicates that the manipulation of NPs ideally in size range of 81–100 nm is favorable for both HY and HER. This might contradict the first impression that the reduction of NPs size significantly enhances the quantum dot effect that subsequently boosts electron transport. However, the preparation and large-scale deployment of small-sized NPs that can stably exist in the cultivation medium has always been a substantial challenge, which will inevitably increase fixing and operating costs. Fortunately, the enhancement of BioH₂ generation seems to be linked to an ideal range of NPs at the size of 81–100 nm; therefore, blindly pursuing small nanoparticles may be meaningless.

5.3. Impact of Other Metal and Non-Metal Nanoparticle Addition

The impact of other metal and non-metal NPs addition upon BioH₂ generation is summarized in Table 3.

Table 3. Comparison of BioH₂ production with the addition of other nanoparticles, where POME: palm oil mill effluent.

NPs	Opt/mg L ⁻¹	Substrate	SC/g L ⁻¹	Size/nm	HY/mmol g ⁻¹	HER/mmol L ⁻¹ h ⁻¹	Reference
Ag	0.002	Glucose	12.5	15	13.8	10.5	[61]
Cu	2.5	Glucose	2.5	97	2.8	5.4	[62]
Pd	5	Glucose	10	100	8.1	6.7	[63]
Au	0.002	Sucrose	15	5	7.5	7.3	[64]
Co	1	Glucose	2.5	100	4.85	0.16	[53]
CoO	1	POME	76.5	17	22.5	0.7	[31]
TiO ₂	100	Xylose	30	30	12	1.8	[47]
ZnO	10	MEG	4	100	7.3	0.58	[51]
MgO	1	Glucose	100	100	4.3	0.1	[53]
Cu/SiO ₂	0.064	Glucose	5	2.5	5.8	0.54	[65]
Ag/SiO ₂	0.107	Glucose	5	2.5	5.4	0.5	[65]
Pd/SiO ₂	0.207	Glucose	5	2.5	5.4	0.52	[65]

The addition of NPs was found to be effective at improving BioH₂ generation due to the fact that NPs can facilitate electron transport in extracellular cultivation medium during fermentation [66,67]. With regard to the HY and HER, it was quite hard to find one individual NPs that positively enhanced both HY and HER simultaneously. This reflects the complex features of the BioH₂ generation process, which generally involves many different steps of sub-metabolic pathways [43,68]. Among the investigated collected literature, CoO-NPs addition was among the most appreciable enhancement for HY and Ag-NPs addition was the most influential factor for HER enhancement. In addition, the impact of adding NPs prepared from hybrid approaches such as combining two different kinds of NPs, i.e., Cu and SiO₂, was marginal. The correlation between BioH₂ generation values (HER and HY) and the corresponding size of the NPs added to the fermentation broth was constructed and is plotted in Figure 5. The corresponding HY and HER varied from 0–30 (mmol g⁻¹) and 0–80 (mmol L⁻¹ h⁻¹), respectively. Regarding to the enhancement of HY, some reported that smaller size (less than 42 nm) surely increased HY from 10 to 20–25 mmol g⁻¹. On the other hand, for the enhancement of HER, some reported that a relatively bigger size of 40–50 nm seemed to significantly increase the H₂ evolution rate. However, by considering the numbers of reports, the majority of works showed (i) the size of NPs seems to be more effective in enhancing HY than HER, and (ii) the rate of H₂ evolution seems to be less responsive to the size of NPs, though some literature reported exceptionally higher values of HER after NPs (40–50 nm) addition.

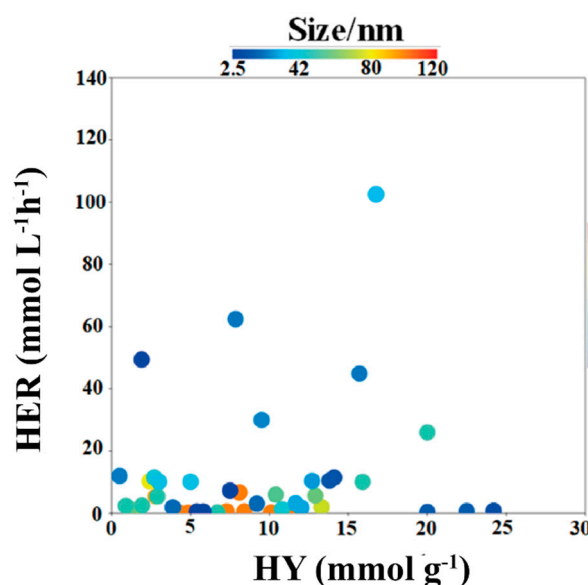


Figure 5. Impact of size of NPs upon HER and HY.

5.4. Impact of Ion Addition

In this work, in order to assess the concentration impacts of different ions upon HY and HER BioH₂ generation, ions including Mg²⁺, Cu²⁺, Na⁺, NH₄⁺, and K⁺ were selected and all data are summarized in Table S1.

It is worth noting that some metal ions inevitably introduced into the culture medium due to the use of NPs addition are not in the scope of discussion. It was quite challenging to find out the detailed concentration ranges in each study due to the factor that many reports did not specify the detailed cultivation steps. Although this could be difficult for estimating the level of those ions during the cultivation, the type of defined and undefined cultivation media used in the studies could be utilized to indirectly estimate the range of those different ions accordingly. The level of different ions upon HY and HER BioH₂ generation are summarized in Tables S2 and 4, respectively, and the collected values from the literature were statistically analyzed through our previously established ANNs-RSM method.

By comparing the p-values, the impact of the variations in ion concentrations upon HY and HER of BioH₂ generation could be identified accordingly [16,69]. It was found that the variations in the investigated ions only statistically influenced HER, but not HY. This suggests pivotal guidance for process intensification for BioH₂ generation. The manipulations of ion concentrations in cultivation media can effectively improve or inhibit the rate but not the potential limit of BioH₂ generation. In other words, the kinetics of BioH₂ generation can be altered by varying some level of ionic concentration. The statistically significant impact of metal ion addition on HER is shown in Figure 6. Among the investigated ions, the single factor included Mg²⁺, Cu²⁺, and Na⁺ (Figure 6A,B) and the combined factor included Mg²⁺/Cu²⁺, Cu²⁺/Na⁺, Na⁺/NH₄⁺, Na⁺/K⁺, and NH₄⁺/K⁺ (Figure 6C–E) as the most influential factors for HER. The responding patterns of HER towards different kinds of ions appeared to be appreciably different. These effects can be broadly classified as counter-effective and synergistic. For instance, for the counter-effective impact, the binary Mg²⁺/Cu²⁺ belongs to this category, as does the binary NH₄⁺/K⁺ (Figure 6A,E). For the synergistic effect, the binary Cu²⁺/Na⁺, Na⁺/NH₄⁺, and Na⁺/K⁺ fall into this category (Figure 6B–D). These different ions will act as essential nutritious elements during metabolism at different stages of the growth of microbes [70–72]. For the growth pattern of microbes, there will normally be lagging, exponential, stationary, and death phases [73–75]. After inoculation, the microbes will experience a lagging phase with different duration [76,77]. The length of the lagging phase depends on many factors, such

as the harshness of cultivation media, which contains lignocellulosic precursors and high levels of salt concentration [78–80].

Table 4. ANOVA analysis for the effect of ion concentration upon HER.

Source	Sum of Squares	DF	Mean Square	F-Value	p-Value
Model	38,286.08	20	1914.30	4.16	0.0005
A-Mg ²⁺	2467.73	1	2467.73	5.36	0.0291
B-Cu ²⁺	1729.50	1	1729.50	3.75	0.0640
C-Na ⁺	7543.84	1	7543.84	16.38	0.0004
D-NH ₄ ⁺	496.57	1	496.57	1.08	0.3091
E-K ⁺	261.49	1	261.49	0.5677	0.4582
AB	7903.35	1	7903.35	17.16	0.0003
AC	1957.27	1	1957.27	4.25	0.0498
AD	513.91	1	513.91	1.12	0.3009
AE	1109.51	1	1109.51	2.41	0.1332
BC	41.84	1	41.84	0.0908	0.7656
BD	330.26	1	330.26	0.7170	0.4052
BE	16.50	1	16.50	0.0358	0.8514
CD	4919.66	1	4919.66	10.68	0.0031
CE	2100.83	1	2100.83	4.56	0.0427
DE	1719.79	1	1719.79	3.73	0.0647
A ²	801.66	1	801.66	1.74	0.1990
B ²	3897.09	1	3897.09	8.46	0.0075
C ²	2148.80	1	2148.80	4.67	0.0406
D ²	387.39	1	387.39	0.8410	0.3679
E ²	1539.54	1	1539.54	3.34	0.0795
Residue	11,515.22	25	460.61		
Lack of fit	11,515.22	20	575.76		
Pure Error	0.0000	5	0.0000		
Cor total	49,801.31	45			

In this table, $r^2 = 0.94$, adjusted $r^2 = 0.93$, predicted $r^2 = 0.93$, and adequate precision (AP) = 15.

The strategies for how to improve and shorten the length of the lagging phase will contribute to the improvement of the duration of the lagging phase [81]. For microbes to initiate their metabolism, elements such as Mg²⁺, Na⁺, NH₄⁺, and K⁺ are essential [82–84]. These elements usually act as the major components of active centers in many enzymes [85–87]. Ensuring a sufficient amount of these necessary elements will facilitate the smooth and fast transition from the lagging phase to the growth phase [88–90]. It is commonly accepted that BioH₂ generation will occur mainly in the exponential and stationary phases [91,92]. Clearly, these investigated literature reports provide useful guidance for the levels of these necessary ion elements in the cultivation media. More importantly, through statistical analysis from our developed ANN-RSM algorithm, the level of the response (the enhanced HER) for those inputs was underpinned. In addition, the order of significance for HER was also identified as the following: Na⁺ > Mg²⁺ > Cu²⁺ > NH₄⁺ > K⁺. From a holistic point of view, all the steps involved in BioH₂ generation metabolism could be targeted as steps to enhance BioH₂ generation (HY and HER). Two major metabolic pathways, namely, butyrate and acetate, are mainly associated with the activities of hydrogenase and the generation of H₂ during dark fermentation [93–95]. From a stoichiometric perspective, the metabolic route towards acetate generates two times that of butyrate pathways [96,97]. From a process intensification point of view, the facilitation of the metabolic pathway towards an acetate pathway is favorable. From our statistical analysis, of all the investigated ions among the literature reports, the yield of BioH₂ generation for these chemical additions of ions is not significant, suggesting that the enhancement of BioH₂ generation by simple chemical additions of ions might be ineffective at further improving the ceiling value of BioH₂ generation yield. For the sake of skewing the delicate balance between butyrate and acetate pathways, the combination of other chemical additions such as acti-

vated carbon, biochars, or porous adsorbents will be more effective in enhancing BioH₂ generation [98–100].

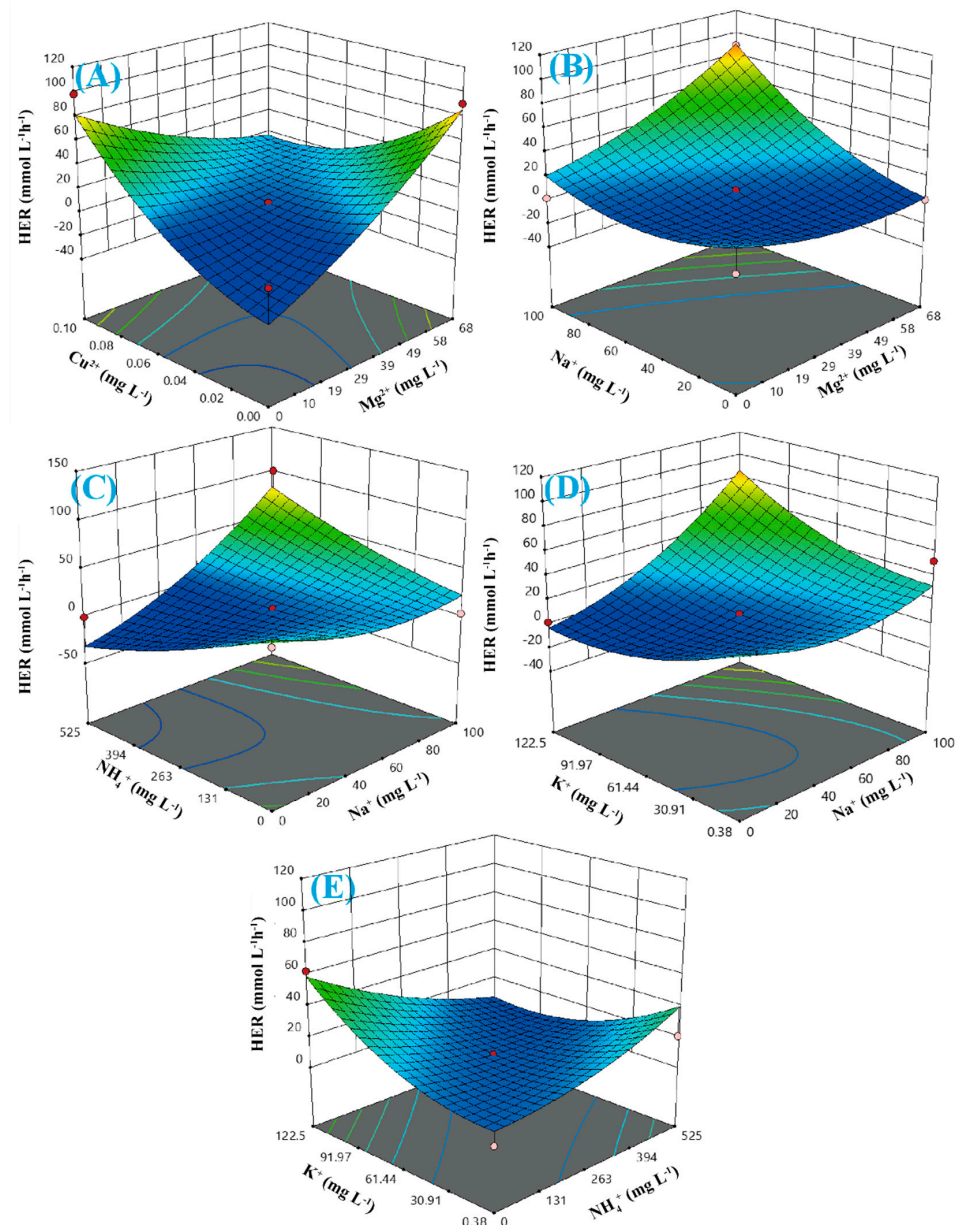


Figure 6. ANNs-RSM analysis of statically significant ion concentrations for HER. (A) Mg²⁺/Cu²⁺ nanoparticle concentration versus HER, (B) Na⁺/Mg²⁺ nanoparticle concentration versus HER, (C) Na⁺/NH₄⁺ nanoparticle concentration versus HER, (D) Na⁺/K⁺ nanoparticle concentration versus HER, (E) NH₄⁺/K⁺ nanoparticle concentration versus HER.

6. Conclusions

The statistical significance of these different NPs and ion additions were rigorously and quantitatively analyzed through a well-developed ANNs-RSM algorithm. As a result, this work provided effective guidance for the size optimization of NP additions and concentration regulation of ion additives in practice. For Fe-based NPs and ions, both the size of NPs and their corresponding concentration are statistically significant to HY. For HER, it was found that the combined effect of NP size and concentration is insignificant to HER. For Ni-based NPs and ions, neither size nor concentration is statistically significant to HY and HER, respectively. The variation in the size of NPs for the enhancement of

HY and HER behaved differently. The smaller (less than 42 nm) were found to definitely improve HY. Simultaneously, for HER, most reported literature indicated that manipulating the size of NPs is ineffective. It was found that variations in the investigated ions only statistically influenced HER, but not HY. This discovery suggests very pivotal guidance for process intensification for BioH₂ generation. Using the constructed algorithm, the level of responses (enhanced HER) towards inputs (other ion additions) was underpinned, and the order of significance towards HER was also identified as the following: Na⁺ > Mg²⁺ > Cu²⁺ > NH₄⁺ > K⁺. However, the number of relevant literature reports is currently limited; with the support of more experimental data, the results predicted by the ANNs-RSM algorithm will be more credible.

Supplementary Materials: The following are available online at <https://www.mdpi.com/article/10.3390/en14185916/s1>, Figure S1: Schematic diagram of methodology: (A) The procedures flowchart, (B) ANNs construction: feed forward three layers networks; Table S1: Ion comparison upon BioH₂ generation—refers to all data missing as, for convenience of calculation, the missing value was replaced by the averaged value during the artificial neuron network learning process; Table S2: ANOVA analysis for the effect of ion concentration on HY, where $r^2 = 0.94$, adjusted $r^2 = 0.93$, predicted $r^2 = 0.93$, and adequate precision (AP) = 15.

Author Contributions: Drafting and data collection, Y.L., J.L. and Y.W.; paper writing and data collection, H.H.; proofreading, S.Y.; programming and modelling, J.H.; supervision, H.J. and T.C.; drafting, G.Y.; funding acquisition and project management, Y.S. All authors have read and agreed to the published version of the manuscript.

Funding: This work was supported by the Key Laboratory of Carbonaceous Wastes Processing and Process Intensification of Zhejiang Province (2020E10018), the Qianjiang Talent Scheme (QJD1803014), the Ningbo Science and Technology Innovation 2025 Key Project (2020Z100), and the Ningbo Municipal Commonweal Key Program (2019C10033 & 2019C10104), UNNC FoSE Researchers Grant 2020 (I01210100011).

Institutional Review Board Statement: Not applicable.

Informed Consent Statement: Not applicable.

Acknowledgments: The authors would like to express their sincere appreciation for the critical and insightful comments raised by anonymous reviewers, which significantly improved the quality of this work.

Conflicts of Interest: The authors declare no conflict of interest.

Abbreviations

ANOVA	Analysis of variation
ANNs	Artificial neural networks
ATR	Auto-thermal reforming
BioH ₂	Biological hydrogen
BBD	Box–Behnken design
CCSU	Carbon capture storage and utilization
CCD	Central composite design
DO	Dissolved oxygen
GHE	Greenhouse gas emission
H ₂	Hydrogen
HER	Hydrogen evolution rate
HY	Hydrogen yield
MSE	Mean square error
NGSR	Natural gas steam reforming
NGTC	Nature gas thermal cracking
NPs	Nanoparticles
RSM	Response surface methodology

References

1. Economist, T. Building up the pillars of state. *The Economist*, 28 March 2020.
2. Bloomberg, Crude Oil (Nymex). In *Bloomberg Energy Index*, 2020/04/06 ed.; Bloomberg: New York, NY, USA, 2020.
3. Carson, R. *Silent Spring*; Houghton Mifflin Harcourt: New York, NY, USA, 1962.
4. Canadell, P.; Quéré, C.L.; Peters, G.; Korsbakken, J.I.; Andrew, R. Eighteen countries showing the way to carbon zero. *The Conversation*, 26 February 2019.
5. Wang, Y.; Tang, M.; Yusuf, A.; Wang, Y.; Zhang, X.; Yang, G.; He, J.; Jin, H.; Sun, Y. Preparation of Catalyst from Phosphorous Rock Using an Improved Wet Process for Transesterification Reaction. *Ind. Eng. Chem. Res.* **2021**, *60*, 22. [[CrossRef](#)]
6. Liu, Z.; Wang, K.; Chen, Y.; Tan, T.; Nielsen, J. Third-generation biorefineries as the means to produce fuels and chemicals from CO₂. *Nat. Catal.* **2020**, *3*, 274–288. [[CrossRef](#)]
7. Glenk, G.; Reichelstein, S. Economics of converting renewable power to hydrogen. *Nat. Energy* **2019**, *4*, 216–222. [[CrossRef](#)]
8. Sun, Y.; He, J.; Yang, G.; Sun, G.; Sage, V. A review of the enhancement of bio-hydrogen generation by chemicals addition. *Catalysts* **2019**, *9*, 353. [[CrossRef](#)]
9. Sun, Y.; Yang, G.; Zhang, L.; Sun, Z. Fischer-Tropsch synthesis in a microchannel reactor using mesoporous silica supported bimetallic Co-Ni catalyst: Process optimization and kinetic modeling. *Chem. Eng. Process. Process. Intensif.* **2017**, *119*, 44–61. [[CrossRef](#)]
10. Sun, Y.; Jia, Z.; Yang, G.; Zhang, L.; Sun, Z. Fischer-Tropsch synthesis using iron based catalyst in a microchannel reactor: Performance evaluation and kinetic modeling. *Int. J. Hydrogen Energy* **2017**, *42*, 29222–29235. [[CrossRef](#)]
11. Sun, Y.; Yang, G.; Wen, C.; Zhang, L.; Sun, Z. Artificial neural networks with response surface methodology for optimization of selective CO₂ hydrogenation using K-promoted iron catalyst in a microchannel reactor. *J. CO₂ Util.* **2018**, *24*, 10–21. [[CrossRef](#)]
12. Sun, Y.; Wang, Y.; He, J.; Yusuf, A.; Wang, Y.; Yang, G.; Xiao, X. Comprehensive kinetic model for acetylene pretreated mesoporous silica supported bimetallic Co-Ni catalyst during Fischer-Tropsch synthesis. *Chem. Eng. Sci.* **2021**, *246*, 116828–116844. [[CrossRef](#)]
13. Wang, Y.X.; Tang, M.; Ling, J.; Wang, Y.; Liu, Y.; Jin, H.; He, J.; Sun, Y. Modeling biohydrogen production using different data driven approaches. *Int. J. Hydrogen Energy* **2021**, *46*, 29822–29833. [[CrossRef](#)]
14. Kumar, G.; Mathimani, T.; Rene, E.R.; Pugazhendhi, A. Application of nanotechnology in dark fermentation for enhanced biohydrogen production using inorganic nanoparticles. *Int. J. Hydrogen Energy* **2019**, *44*, 13106–13113. [[CrossRef](#)]
15. Wang, Y.; Yang, G.; Sage, V.; Xu, J.; Sun, G.; He, J.; Sun, Y. Optimization of dark fermentation for biohydrogen production using a hybrid artificial neural network (ANN) and response surface methodology (RSM) approach. *Environ. Prog. Sustain. Energy* **2021**, *40*, e13485. [[CrossRef](#)]
16. Sun, Y.; Yang, G.; Xu, M.; Xu, J.; Sun, Z. A simple coupled ANNs-RSM approach in modeling product distribution of Fischer—Tropsch synthesis using a microchannel reactor with Ru-promoted Co/Al₂O₃ catalyst. *Int. J. Energy Res.* **2020**, *44*, 1046–1061. [[CrossRef](#)]
17. Gadhe, A.; Sonawane, S.S.; Varma, M.N. Enhancement effect of hematite and nickel nanoparticles on biohydrogen production from dairy wastewater. *Int. J. Hydrogen Energy* **2015**, *40*, 4502–4511. [[CrossRef](#)]
18. Taherdanak, M.; Zilouei, H.; Karimi, K. Investigating the effects of iron and nickel nanoparticles on dark hydrogen fermentation from starch using central composite design. *Int. J. Hydrogen Energy* **2015**, *40*, 12956–12963. [[CrossRef](#)]
19. Trofanchuk, O.; Stein, M.; Geßner, C.; Lenzian, F.; Higuchi, Y.; Lubitz, W. Single crystal EPR studies of the oxidized active site of [NiFe] hydrogenase from *Desulfovibrio vulgaris* Miyazaki F. *JBC J. Biol. Inorg. Chem.* **2000**, *5*, 36–44. [[CrossRef](#)]
20. Morra, S.; Arizzi, M.; Allegra, P.; La Licata, B.; Sagnelli, F.; Zitella, P.; Gilardi, G.; Valetti, F. Expression of different types of [FeFe]-hydrogenase genes in bacteria isolated from a population of a bio-hydrogen pilot-scale plant. *Int. J. Hydrogen Energy* **2014**, *39*, 9018–9027. [[CrossRef](#)]
21. Peters, J.W.; Schut, G.J.; Boyd, E.S.; Mulder, D.W.; Shepard, E.M.; Broderick, J.B.; King, P.W.; Adams, M.W. [FeFe]- and [NiFe]-hydrogenase diversity, mechanism, and maturation. *Biochim. Biophys. Acta (BBA)-Mol. Cell Res.* **2015**, *1853*, 1350–1369. [[CrossRef](#)]
22. Kothari, R.; Singh, D.; Tyagi, V.; Tyagi, S. Fermentative hydrogen production—An alternative clean energy source. *Renew. Sustain. Energy Rev.* **2012**, *16*, 2337–2346. [[CrossRef](#)]
23. Elreedy, A.; Ibrahim, E.; Hassan, N.; El-Dissouky, A.; Fujii, M.; Yoshimura, C.; Tawfik, A. Nickel-graphene nanocomposite as a novel supplement for enhancement of biohydrogen production from industrial wastewater containing mono-ethylene glycol. *Energy Convers. Manag.* **2017**, *140*, 133–144. [[CrossRef](#)]
24. Pohorelic, B.K.; Voordouw, J.K.; Lojou, E.; Dolla, A.; Harder, J.; Voordouw, G. Effects of deletion of genes encoding Fe-only hydrogenase of *Desulfovibrio vulgaris* Hildenborough on hydrogen and lactate metabolism. *J. Bacteriol.* **2002**, *184*, 679–686. [[CrossRef](#)] [[PubMed](#)]
25. Vignais, P.M.; Billoud, B. Occurrence, classification, and biological function of hydrogenases: An overview. *Chem. Rev.* **2007**, *107*, 4206–4272. [[CrossRef](#)]
26. Kucharska, K.; Hołowacz, I.; Konopacka-Lyskawa, D.; Rybarczyk, P.; Kamiński, M. Key issues in modeling and optimization of lignocellulosic biomass fermentative conversion to gaseous biofuels. *Renew. Energy* **2018**, *129*, 384–408. [[CrossRef](#)]
27. Mohanraj, S.; Kodhaiyolii, S.; Rengasamy, M.; Pugalenti, V. Phytosynthesized iron oxide nanoparticles and ferrous iron on fermentative hydrogen production using *Enterobacter cloacae*: Evaluation and comparison of the effects. *Int. J. Hydrogen Energy* **2014**, *39*, 11920–11929. [[CrossRef](#)]
28. Mohanraj, S.; Kodhaiyolii, S.; Rengasamy, M.; Pugalenti, V. Green synthesized iron oxide nanoparticles effect on fermentative hydrogen production by *Clostridium acetobutylicum*. *Appl. Biochem. Biotechnol.* **2014**, *173*, 318–331. [[CrossRef](#)] [[PubMed](#)]

29. Patel, S.K.; Lee, J.-K.; Kalia, V.C. Nanoparticles in biological hydrogen production: An overview. *Indian J. Microbiol.* **2018**, *58*, 8–18. [[CrossRef](#)] [[PubMed](#)]
30. Gadhe, A.; Sonawane, S.S.; Varma, M.N. Influence of nickel and hematite nanoparticle powder on the production of biohydrogen from complex distillery wastewater in batch fermentation. *Int. J. Hydrogen Energy* **2015**, *40*, 10734–10743. [[CrossRef](#)]
31. Mishra, P.; Thakur, S.; Mahapatra, D.M.; Ab Wahid, Z.; Liu, H.; Singh, L. Impacts of nano-metal oxides on hydrogen production in anaerobic digestion of palm oil mill effluent—A novel approach. *Int. J. Hydrogen Energy* **2018**, *43*, 2666–2676. [[CrossRef](#)]
32. Sun, Y.; Yang, G.; Zhang, J.; Wen, C.; Sun, Z. Optimization and kinetic modeling of an enhanced bio-hydrogen fermentation with the addition of synergistic biochar and nickel nanoparticle. *Int. J. Energy Res.* **2019**, *43*, 983–999. [[CrossRef](#)]
33. Kodhaiyolii, S.; Mohanraj, S.; Rengasamy, M.; Pugalenth, V. Phytofabrication of bimetallic Co–Ni nanoparticles using *Boerhavia diffusa* leaf extract: Analysis of phytochemicals and application for simultaneous production of biohydrogen and bioethanol. *Mater. Res. Express* **2019**, *6*, 095051. [[CrossRef](#)]
34. Jiang, X.C.; Hu, J.S.; Lieber, A.M.; Jackan, C.S.; Biffinger, J.C.; Fitzgerald, L.A.; Ringeisen, B.R.; Lieber, C.M. Nanoparticle Facilitated Extracellular Electron Transfer in Microbial Fuel Cells. *Nano Lett.* **2014**, *14*, 6737–6742. [[CrossRef](#)]
35. El-Naggar, M.Y.; Wanger, G.; Leung, K.M.; Yuzvinsky, T.D.; Southam, G.; Yang, J.; Lau, W.M.; Neelson, K.H.; Gorby, Y.A. Electrical transport along bacterial nanowires from *Shewanella oneidensis* MR-1. *Proc. Natl. Acad. Sci. USA* **2010**, *107*, 18127–18131. [[CrossRef](#)]
36. Viggi, C.C.; Rossetti, S.; Fazi, S.; Paiano, P.; Majone, M.; Aulenta, F. Magnetite Particles Triggering a Faster and More Robust Syntrophic Pathway of Methanogenic Propionate Degradation. *Environ. Sci. Technol.* **2014**, *48*, 7536–7543. [[CrossRef](#)]
37. Wang, J.; Wan, W. Effect of Fe²⁺ concentration on fermentative hydrogen production by mixed cultures. *Int. J. Hydrogen Energy* **2008**, *33*, 1215–1220. [[CrossRef](#)]
38. Frey, M. Hydrogenases: Hydroge—activating enzymes. *ChemBioChem* **2002**, *3*, 153–160. [[CrossRef](#)]
39. Shanmugam, S.; Hari, A.; Pandey, A.; Mathimani, T.; Felix, L.; Pugazhendhi, A. Comprehensive review on the application of inorganic and organic nanoparticles for enhancing biohydrogen production. *Fuel* **2020**, *270*, 117453. [[CrossRef](#)]
40. Nadeem, F.; Jiang, D.; Tahir, N.; Alam, M.; Zhang, Z.; Yi, W.; Chaoyang, L.; Zhang, Q. Defect engineering in SnO₂ nanomaterials: Pathway to enhance the biohydrogen production from agricultural residue of corn stover. *Appl. Mater. Today* **2020**, *21*, 100850. [[CrossRef](#)]
41. Shanmugam, S.; Krishnaswamy, S.; Chandrababu, R.; Veerabagu, U.; Pugazhendhi, A.; Mathimani, T. Optimal immobilization of *Trichoderma asperellum* laccase on polymer coated Fe₃O₄@SiO₂ nanoparticles for enhanced biohydrogen production from delignified lignocellulosic biomass. *Fuel* **2020**, *273*, 117777. [[CrossRef](#)]
42. Braga, J.K.; Stancari, R.A.; Motteran, F.; Malavazi, I.; Varesche, M.B.A. Metals addition for enhanced hydrogen, acetic and butyric acids production from cellulosic substrates by *Clostridium butyricum*. *Biomass Bioenergy* **2021**, *150*, 105679. [[CrossRef](#)]
43. Bhatia, S.K.; Jagtap, S.S.; Bedekar, A.A.; Bhatia, R.K.; Rajendran, K.; Pugazhendhi, A.; Rao, C.V.; Atabani, A.; Kumar, G.; Yang, Y.-H. Renewable biohydrogen production from lignocellulosic biomass using fermentation and integration of systems with other energy generation technologies. *Sci. Total Environ.* **2020**, *765*, 144429. [[CrossRef](#)]
44. Wang, J.; Wan, W. Influence of Ni²⁺ concentration on biohydrogen production. *Bioresour. Technol.* **2008**, *99*, 8864–8868. [[CrossRef](#)]
45. Yang, G.; Wang, J. Improving mechanisms of biohydrogen production from grass using zero-valent iron nanoparticles. *Bioresour. Technol.* **2018**, *266*, 413–420. [[CrossRef](#)]
46. Dolly, S.; Pandey, A.; Pandey, B.K.; Gopal, R. Process parameter optimization and enhancement of photo-biohydrogen production by mixed culture of *Rhodospirillum rubrum* NMBL-02 and *Escherichia coli* NMBL-04 using Fe-nanoparticle. *Int. J. Hydrogen Energy* **2015**, *40*, 16010–16020. [[CrossRef](#)]
47. Hsieh, P.-H.; Lai, Y.-C.; Chen, K.-Y.; Hung, C.-H. Explore the possible effect of TiO₂ and magnetic hematite nanoparticle addition on biohydrogen production by *Clostridium pasteurianum* based on gene expression measurements. *Int. J. Hydrogen Energy* **2016**, *41*, 21685–21691. [[CrossRef](#)]
48. Yin, Y.; Wang, J. Enhanced biohydrogen production from macroalgae by zero-valent iron nanoparticles: Insights into microbial and metabolites distribution. *Bioresour. Technol.* **2019**, *282*, 110–117. [[CrossRef](#)] [[PubMed](#)]
49. Engliman, N.S.; Abdul, P.M.; Wu, S.-Y.; Jahim, J.M. Influence of iron (II) oxide nanoparticle on biohydrogen production in thermophilic mixed fermentation. *Int. J. Hydrogen Energy* **2017**, *42*, 27482–27493. [[CrossRef](#)]
50. Malik, S.N.; Pugalenth, V.; Vaidya, A.N.; Ghosh, P.C.; Mudliar, S.N. Kinetics of nano-catalysed dark fermentative hydrogen production from distillery wastewater. *Energy Procedia* **2014**, *54*, 417–430. [[CrossRef](#)]
51. Elreedy, A.; Fujii, M.; Koyama, M.; Nakasaki, K.; Tawfik, A. Enhanced fermentative hydrogen production from industrial wastewater using mixed culture bacteria incorporated with iron, nickel, and zinc-based nanoparticles. *Water Res.* **2019**, *151*, 349–361. [[CrossRef](#)]
52. Lin, R.; Cheng, J.; Ding, L.; Song, W.; Liu, M.; Zhou, J.; Cen, K. Enhanced dark hydrogen fermentation by addition of ferric oxide nanoparticles using *Enterobacter aerogenes*. *Bioresour. Technol.* **2016**, *207*, 213–219. [[CrossRef](#)] [[PubMed](#)]
53. Zaidi, A.A.; RuiZhe, F.; Shi, Y.; Khan, S.Z.; Mushtaq, K. Nanoparticles augmentation on biogas yield from microalgal biomass anaerobic digestion. *Int. J. Hydrogen Energy* **2018**, *43*, 14202–14213. [[CrossRef](#)]
54. Wang, J.; Wan, W. The effect of substrate concentration on biohydrogen production by using kinetic models. *Sci. China Ser. B Chem.* **2008**, *51*, 1110–1117. [[CrossRef](#)]

55. Reddy, K.; Nasr, M.; Kumari, S.; Kumar, S.; Gupta, S.K.; Enitan, A.M.; Bux, F. Biohydrogen production from sugarcane bagasse hydrolysate: Effects of pH, S/X, Fe²⁺, and magnetite nanoparticles. *Environ. Sci. Pollut. Res.* **2017**, *24*, 8790–8804. [[CrossRef](#)]
56. Han, H.; Cui, M.; Wei, L.; Yang, H.; Shen, J. Enhancement effect of hematite nanoparticles on fermentative hydrogen production. *Bioresour. Technol.* **2011**, *102*, 7903–7909. [[CrossRef](#)]
57. Mullai, P.; Yogeswari, M.; Sridevi, K. Optimisation and enhancement of biohydrogen production using nickel nanoparticles—A novel approach. *Bioresour. Technol.* **2013**, *141*, 212–219. [[CrossRef](#)]
58. Taherdanak, M.; Zilouei, H.; Karimi, K. The effects of Fe⁰ and Ni⁰ nanoparticles versus Fe²⁺ and Ni²⁺ ions on dark hydrogen fermentation. *Int. J. Hydrogen Energy* **2016**, *41*, 167–173. [[CrossRef](#)]
59. Sun, Y.; Wang, Y.; Yang, G.; Sun, Z. Optimization of biohydrogen production using acid pretreated corn stover hydrolysate followed by nickel nanoparticle addition. *Int. J. Energy Res.* **2020**, *44*, 1843–1857. [[CrossRef](#)]
60. Zhang, J.; Zhao, W.; Yang, J.; Li, Z.; Zhang, J.; Zang, L. Comparison of mesophilic and thermophilic dark fermentation with nickel ferrite nanoparticles supplementation for biohydrogen production. *Bioresour. Technol.* **2021**, *329*, 124853. [[CrossRef](#)]
61. Zhao, W.; Zhang, Y.; Du, B.; Wei, D.; Wei, Q.; Zhao, Y. Enhancement effect of silver nanoparticles on fermentative biohydrogen production using mixed bacteria. *Bioresour. Technol.* **2013**, *142*, 240–245. [[CrossRef](#)] [[PubMed](#)]
62. Mohanraj, S.; Anbalagan, K.; Rajaguru, P.; Pugalanthi, V. Effects of phytogetic copper nanoparticles on fermentative hydrogen production by *Enterobacter cloacae* and *Clostridium acetobutylicum*. *Int. J. Hydrogen Energy* **2016**, *41*, 10639–10645. [[CrossRef](#)]
63. Mohanraj, S.; Anbalagan, K.; Kodhaiyolii, S.; Pugalanthi, V. Comparative evaluation of fermentative hydrogen production using *Enterobacter cloacae* and mixed culture: Effect of Pd (II) ion and phytogetic palladium nanoparticles. *J. Biotechnol.* **2014**, *192*, 87–95. [[CrossRef](#)] [[PubMed](#)]
64. Zhang, Y.; Shen, J. Enhancement effect of gold nanoparticles on biohydrogen production from artificial wastewater. *Int. J. Hydrogen Energy* **2007**, *32*, 17–23. [[CrossRef](#)]
65. Beckers, L.; Hiligsmann, S.; Lambert, S.D.; Heinrichs, B.; Thonart, P. Improving effect of metal and oxide nanoparticles encapsulated in porous silica on fermentative biohydrogen production by *Clostridium butyricum*. *Bioresour. Technol.* **2013**, *133*, 109–117. [[CrossRef](#)] [[PubMed](#)]
66. Ameen, F.; Alsamhary, K.; Alabdullatif, J.A.; ALNadhari, S. A review on metal-based nanoparticles and their toxicity to beneficial soil bacteria and fungi. *Ecotoxicol. Environ. Saf.* **2021**, *213*, 112027. [[CrossRef](#)]
67. Pu, Y.; Laratte, B.; Marks, R.S.; Ionescu, R.E. Impact of copper nanoparticles on porcine neutrophils: Ultrasensitive characterization factor combining chemiluminescence information and USEtox assessment model. *Mater. Today Commun.* **2017**, *11*, 68–75. [[CrossRef](#)]
68. El-Dalatony, M.M.; Zheng, Y.; Ji, M.-K.; Li, X.; Salama, E.-S. Metabolic pathways for microalgal biohydrogen production: Current progress and future perspectives. *Bioresour. Technol.* **2020**, *318*, 124253. [[CrossRef](#)]
69. Sun, Y.; Yang, G.; Zhang, L.; Sun, Z. Fischer-Tropsch synthesis using iron-based catalyst in a microchannel reactor: Hybrid lump kinetic with ANNs/RSM. *Chem. Eng. Process. Process. Intensif.* **2017**, *122*, 181–189. [[CrossRef](#)]
70. Rambabu, K.; Show, P.-L.; Bharath, G.; Banat, F.; Naushad, M.; Chang, J.-S. Enhanced biohydrogen production from date seeds by *Clostridium thermocellum* ATCC 27405. *Int. J. Hydrogen Energy* **2020**, *45*, 22271–22280. [[CrossRef](#)]
71. Ulhiza, T.A.; Puad, N.I.M.; Azmi, A.S. Optimization of culture conditions for biohydrogen production from sago wastewater by *Enterobacter aerogenes* using Response Surface Methodology. *Int. J. Hydrogen Energy* **2018**, *43*, 22148–22158. [[CrossRef](#)]
72. Zainal, B.S.; Zinatizadeh, A.A.; Chyuan, O.H.; Mohd, N.S.; Ibrahim, S. Effects of process, operational and environmental variables on biohydrogen production using palm oil mill effluent (POME). *Int. J. Hydrogen Energy* **2018**, *43*, 10637–10644. [[CrossRef](#)]
73. Usman, M.; Kavitha, S.; Kannah, Y.; Yogalakshmi, K.; Sivashanmugam, P.; Bhatnagar, A.; Kumar, G. A critical review on limitations and enhancement strategies associated with biohydrogen production. *Int. J. Hydrogen Energy* **2021**, *46*, 31.
74. Sethupathy, A.; Kumar, P.S.; Sivashanmugam, P.; Arun, C.; Banu, J.R.; Ashokkumar, M. Evaluation of biohydrogen production potential of fragmented sugar industry biosludge using ultrasonication coupled with egtazic acid. *Int. J. Hydrogen Energy* **2021**, *46*, 1705–1714. [[CrossRef](#)]
75. Mirza, S.S.; Qazi, J.I.; Liang, Y.; Chen, S. Growth characteristics and photofermentative biohydrogen production potential of purple non sulfur bacteria from sugar cane bagasse. *Fuel* **2019**, *255*, 115805. [[CrossRef](#)]
76. Urbaniec, K.; Bakker, R.R. Biomass residues as raw material for dark hydrogen fermentation—A review. *Int. J. Hydrogen Energy* **2015**, *40*, 3648–3658. [[CrossRef](#)]
77. Hu, J.; Nagarajan, D.; Zhang, Q.; Chang, J.-S.; Lee, D.-J. Heterotrophic cultivation of microalgae for pigment production: A review. *Biotechnol. Adv.* **2018**, *36*, 54–67. [[CrossRef](#)]
78. Sun, Y.; Mang, J.-P.; Yang, G.; Li, Z.-H. Study on the spectra of spruce lignin with chlorine dioxide oxidation. *Spectrochim. Acta Part A Mol. Spectrosc.* **2007**, *27*, 1551–1554.
79. Tan, M.; Ma, L.; Rehman, M.S.U.; Ahmed, M.A.; Sajid, M.; Xu, X.; Sun, Y.; Cui, P.; Xu, J. Screening of acidic and alkaline pretreatments for walnut shell and corn stover biorefining using two way heterogeneity evaluation. *Renew. Energy* **2019**, *132*, 950–958. [[CrossRef](#)]
80. Meghana, M.; Shastri, Y. Sustainable valorization of sugar industry waste: Status, opportunities, and challenges. *Bioresour. Technol.* **2020**, *303*, 122929. [[CrossRef](#)]
81. Shuler, M.L. *Bioprocess Engineering: Basic Concepts*; Prentice-Hall: New York, NY, USA, 2017; pp. 412–420.

82. Zhao, X.; Xing, D.; Qi, N.; Zhao, Y.; Hu, X.; Ren, N. Deeply mechanism analysis of hydrogen production enhancement of *Ethanoligenens harbinense* by Fe^{2+} and Mg^{2+} : Monitoring at growth and transcription levels. *Int. J. Hydrogen Energy* **2017**, *42*, 19695–19700. [[CrossRef](#)]
83. Palomo-Briones, R.; Razo-Flores, E.; Bernet, N.; Trably, E. Dark-fermentative biohydrogen pathways and microbial networks in continuous stirred tank reactors: Novel insights on their control. *Appl. Energy* **2017**, *198*, 77–87. [[CrossRef](#)]
84. Wimonsong, P.; Llorca, J.; Nitorisavut, R. Catalytic activity and characterization of Fe–Zn–Mg–Al hydrotalcites in biohydrogen production. *Int. J. Hydrogen Energy* **2013**, *38*, 10284–10292. [[CrossRef](#)]
85. Woodward, J.; Orr, M.; Cordray, K.; Greenbaum, E. Enzymatic production of biohydrogen. *Nature* **2000**, *405*, 1014–1015. [[CrossRef](#)]
86. Ergal, I.; Gräf, O.; Hasibar, B.; Steiner, M.; Vukotić, S.; Bochmann, G.; Fuchs, W.; Simon, K.-M.R. Biohydrogen production beyond the Thauer limit by precision design of artificial microbial consortia. *Commun. Biol.* **2020**, *3*, 1–12. [[CrossRef](#)]
87. Wang, S.; Tang, H.; Peng, F.; Yu, X.; Su, H.; Xu, P.; Tan, T. Metabolite-based mutualism enhances hydrogen production in a two-species microbial consortium. *Commun. Biol.* **2019**, *2*, 1–11. [[CrossRef](#)]
88. Lu, Y.; Zhao, H.; Zhang, C.; Xing, X.-H. Insights into the global regulation of anaerobic metabolism for improved biohydrogen production. *Bioresour. Technol.* **2016**, *200*, 35–41. [[CrossRef](#)] [[PubMed](#)]
89. Banu, J.R.; Ginni, G.; Kavitha, S.; Kannah, R.Y.; Kumar, S.A.; Bhatia, S.K.; Kumar, G. Integrated biorefinery routes of biohydrogen: Possible utilization of acidogenic fermentative effluent. *Bioresour. Technol.* **2021**, *319*, 124241. [[CrossRef](#)] [[PubMed](#)]
90. Wang, L. *Sustainable Bioenergy Production*; CRC Press: Boca Raton, FL, USA, 2019.
91. Banu, J.R.; Kavitha, S.; Kannah, R.Y.; Bhosale, R.R.; Kumar, G. Industrial wastewater to biohydrogen: Possibilities towards successful biorefinery route. *Bioresour. Technol.* **2020**, *298*, 122378. [[CrossRef](#)] [[PubMed](#)]
92. Nawaz, M.Z.; Bilal, M.; Tariq, A.; Iqbal, H.M.; Alghamdi, H.A.; Cheng, H. Bio-purification of sugar industry wastewater and production of high-value industrial products with a zero-waste concept. *Crit. Rev. Food Sci. Nutr.* **2020**, 1–18. [[CrossRef](#)] [[PubMed](#)]
93. Liu, D.; Sun, Y.; Li, Y.; Lu, Y. Perturbation of formate pathway and NADH pathway acting on the biohydrogen production. *Sci. Rep.* **2017**, *7*, 1–8.
94. Gutekunst, K.; Hoffmann, D.; Westernströer, U.; Schulz, R.; Garbe-Schönberg, D.; Appel, J. In-vivo turnover frequency of the cyanobacterial NiFe-hydrogenase during photohydrogen production outperforms in-vitro systems. *Sci. Rep.* **2018**, *8*, 1–10.
95. Mangayil, R.; Karp, M.; Lamminmäki, U.; Santala, V. Recombinant antibodies for specific detection of clostridial [Fe-Fe] hydrogenases. *Sci. Rep.* **2016**, *6*, 1–9. [[CrossRef](#)]
96. Oladokun, O.; Ahmad, A.; Abdullah, T.A.T.; Nyakuma, B.B.; Kamaroddin, M.F.A.; Nor, S.H.M. Biohydrogen production from *Imperata cylindrica* bio-oil using non-stoichiometric and thermodynamic model. *Int. J. Hydrogen Energy* **2017**, *42*, 9011–9023. [[CrossRef](#)]
97. Show, K.-Y.; Lee, D.-J.; Chang, J.-S. Bioreactor and process design for biohydrogen production. *Bioresour. Technol.* **2011**, *102*, 8524–8533. [[CrossRef](#)] [[PubMed](#)]
98. Wang, Y.; Yang, G.; He, J.; Sun, G.; Sun, Z.; Sun, Y. Preparation of biochar catalyst from black liquor by spray drying and fluidized bed carbonation for biodiesel synthesis. *Process. Saf. Environ. Prot.* **2020**, *141*, 333–343. [[CrossRef](#)]
99. Park, J.-H.; Kim, D.-H.; Kim, H.-S.; Wells, G.F.; Park, H.-D. Granular activated carbon supplementation alters the metabolic flux of *Clostridium butyricum* for enhanced biohydrogen production. *Bioresour. Technol.* **2019**, *281*, 318–325. [[CrossRef](#)] [[PubMed](#)]
100. Jamali, N.S.; Jahim, J.M.; Isahak, W.N.R.W.; Abdul, P.M. Particle size variations of activated carbon on biofilm formation in thermophilic biohydrogen production from palm oil mill effluent. *Energy Convers. Manag.* **2017**, *141*, 354–366. [[CrossRef](#)]